Tunable and enhanced Rashba spin-orbit coupling in iridate-manganite heterostructures

T. S. Suraj,[1,2,*] Ganesh Ji Omar,[3,4,*] Hariom Jani,[4,6] M. M. Juvaid,[1,3,4] Sonu Hooda,[4] Anindita Chaudhuri,[5] Andrivo Rusydi,[3,5] K. Sethupathi,[2] Thirumalai Venkatesan,[3,4,6,7] Ariando Ariando,[3,4,6,†] and M. S. Ramachandra Rao[1,‡]

[1]*Department of Physics, Nano Functional Materials Technology Center, Material Science Research Center, Indian Institute of Technology Madras, Chennai 600036, India*

[2]*Low Temperature Physics Lab, Department of Physics, Indian Institute of Technology Madras, Chennai 600036, India*

[3]*Department of Physics, National University of Singapore, Singapore 117542, Singapore*

[4]*NUSNNI-NanoCore, National University of Singapore, Singapore 117411, Singapore*

[5]*Singapore Synchrotron Light Source, National University of Singapore, 5 Research Link, Singapore 117603, Singapore*

[6]*National University of Singapore Graduate School for Integrative Sciences and Engineering (NGS), University Hall, 21 Lower Kent Ridge Road, Singapore 119077, Singapore*

[7]*Department of Electrical and Computer Engineering, National University of Singapore, Singapore 117576, Singapore*

(Received 31 March 2020; revised 30 August 2020; accepted 2 September 2020; published 25 September 2020)

Tailoring spin-orbit interactions and Coulomb repulsion are the key features to observe exotic physical phenomena such as magnetic anisotropy and topological spin texture at oxide interfaces. Our study proposes a platform for engineering magnetism and spin-orbit coupling at the $LaMnO_3/SrIrO_3$ ($3d$-$5d$) oxide interface by tuning the $LaMnO_3$ growth conditions, which controls the lattice displacement and spin-correlated interfacial coupling through charge transfer. We report a tunable and enhanced interface-induced Rashba spin-orbit coupling where the spin relaxation mechanism varies with magnetic behavior of the underlying $LaMnO_3$ layer. The x-ray spectroscopy measurements reveal the quantitative valence states of Mn and their impact on charge transfer. Our angle-dependent magnetoresistance measurements also reflects the signature of magnetic proximity effect in $SrIrO_3$ and can be tuned with the magnetic nature of $LaMnO_3$ in a $LaMnO_3/SrIrO_3$ bilayer. Our work demonstrates a route to engineer the interface-induced Rashba spin-orbit coupling and magnetic proximity effect at the $3d$-$5d$ oxide interface for spintronics applications.

DOI: 10.1103/PhysRevB.102.125145

I. INTRODUCTION

The combination of artificially layered complex oxides in heterostructures opens the possibility of realizing novel functional properties from the strong interplay among charge, spin, orbit, and lattice degrees of freedom which might be absent in the constituent oxide layers. Moreover, the interfacial effects mediated through charge transfer between oxide layers play a significant role in tuning the interface physics and its resultant properties [1–6]. Among oxides, there is a surge in research interest for combinations of $3d$-$5d$ oxide interfaces for exploring various phenomena, such as manipulation of spin-orbit coupling that has potential applications in spintronics memory devices [7–9]. Among $5d$ oxide materials, iridates are the most exciting due to the combination of large intrinsic spin-orbit coupling (interaction strength; ξ) and their tunable Coulombic correlations (interaction strength, U) [10]. The strong spin-orbit coupling in the $5d$ orbital state splits the t_{2g} levels due to crystal field into a fully filled $J_{\text{eff}}= \frac{3}{2}$ quartet and the $J_{\text{eff}}= \frac{1}{2}$ doublet having a single electron (hole) forming a half-filled band. Depending on the interaction strength (U), an iridate system can become a Mott insulator or it can be driven to have a metallic/semimetallic ground state [11–13]. Perovskite $SrIrO_3$ can be epitaxially grown over various transition metal oxides (TMOs) and its semimetallicity can be tuned by compressive strain and reduced dimensionality, which makes it an ideal choice as $5d$ oxide layers in $3d$-$5d$ heterostructures [14–16].

On the other hand, $LaMnO_3$ is the parent compound for manganite, containing the $3d$ element Mn, which is an A-type antiferromagnetic insulator in bulk and could behave like a ferromagnet in epitaxial thin films due to vacancies or epitaxial strain [17–19]. Our earlier studies demonstrated the origin of ferromagnetism in $LaMnO_3/SrTiO_3$ heterostructures by mapping the magnetic domains which show long-range ferromagnetic ordering arising from electron doping at the $LaMnO_3/SrTiO_3$ due to polar catastrophe [20]. $LaMnO_3$ thin films grown under different deposition oxygen partial pressures (pO_2) have also been systematically studied by different groups with a variety of experimental techniques such as x-ray absorption spectroscopy (XAS), x-ray magnetic circular dichroism, and transmission electron microscopy-electron energy loss spectroscopy [19–24]. Roqueta *et al.* reported tunability of strain-controlled ferromagnetism in $LaMnO_3$ during growth by varying the background pO_2 that resulted in a rich magnetic phase diagram. However, the oxygen nonstoichiometry creates an imbalance in Mn valence states by

*These authors contributed equally to this work.
†ariando@nus.edu.sg
‡msrrao@iitm.ac.in

charge ordering, which induces double exchange mediated ferromagnetism in $LaMnO_3$ [21]. This aspect of oxygen non-stoichiometry tuning to control spin-orbit interactions via a 3*d*-5*d* interface has hitherto not been explored.

The interaction of TMOs with $SrIrO_3$ exhibited very interesting properties, for example, tuning magnetic anisotropy in $La_{1-x}Sr_xMnO_3/SrIrO_3$ superlattices through octahedral rotation [25,26] and inducing a metal-insulator transition in $LaNiO_3$ by charge transfer from $SrIrO_3$ [27]. Magnetic phases such as spin glass and skyrmions in $SrRuO_3/SrIrO_3$ superlattices were also reported [28]. The interfacial charge-transfer-driven phenomena like the emergence of magnetism in $SrIrO_3/SrMnO_3$ superlattices [1,29] and interfacial re-entrant spin/super spin-glass states have been reported recently in $LaMnO_3/SrIrO_3$ bilayers [30].

In this paper, we demonstrate the influence of $LaMnO_3$ layers on magnetotransport and spin-orbit coupling properties at the $SrIrO_3$ interface where the $LaMnO_3$ growth condition plays a major role. Our magnetotransport measurements show a tunable and enhanced Rashba spin-orbit coupling at the interface with varying magnetic behaviors of $LaMnO_3$. In addition, x-ray photoelectron spectroscopy (XPS) measurements indicate different fractions of Mn^{3+} and Mn^{4+} valence states in $LaMnO_3$ grown at different oxygen partial pressures; this affects the spin-orbit-coupling-related parameters at the $LaMnO_3/SrIrO_3$ interface. Also, interfacial charge transfer from Ir^{4+} to Mn^{3+} and Mn^{4+} from growth variation has not been reported at a 3*d*-5*d* interface, where as individual (Mn^{3+}) $LaMnO_3/SrIrO_3$ [30] and (Mn^{4+}) $SrMnO_3/SrIrO_3$ interface charge transfers have been reported earlier [1,29].

Spin Hall magnetoresistance (SMR) has become a versatile tool to probe the nature of magnetic interfaces [31,32]. In our case, $LaMnO_3$ is a magnetic layer and $SrIrO_3$ is a metallic oxide with large spin-orbit coupling [32]. Although $SrIrO_3$ is the best choice for spin-transport studies due to low charge conductivity and large spin-orbit coupling, it has not been thoroughly explored through electrical transport measurements [33]. The angle-dependent magnetoresistance (ADMR) measurements showed signatures of magnetic proximity effect (MPE) in $SrIrO_3$, which is reflected in ADMR magnitude as well. Our study provides a platform for tuning interfacial effects in TMO heterostructures by interface modifications, which may have an impact on designing spintronic devices with an emerging 5*d* quantum material.

II. RESULTS AND DISCUSSION

$LaMnO_3$ thin films were grown on (001) oriented $(LaAlO_3)_{0.3}(Sr_2TaAlO_6)_{0.7}$ (LSAT) substrates by pulsed laser deposition (PLD) to rule out the possibility of polar catastrophe and minimize lattice mismatch. LP-LMO denotes 10-nm-thick $LaMnO_3$ grown at low pO_2 (37.5×10^{-3} mTorr); similarly, HP-LMO denotes 10-nm-thick $LaMnO_3$ grown at high pO_2 (37.5 mTorr). The $LaMnO_3/SrIrO_3$ bilayers with 5-nm-thick $SrIrO_3$ deposited on top of HP- and LP-LMO under similar conditions (deposition $pO_2 = 100$ mTorr) are labeled as LP-/HP-LMO-SIO, respectively, the detailed growth-related procedure can be found in the Supplemental Material (SM) [34]. The quality of PLD-grown LP/HP-LMO samples are confirmed by atomic force microscopy (AFM), x-ray diffraction (XRD) and x-ray reflectivity studies (see SM [34]).

The electrical and magnetotransport properties of the samples are investigated using the physical property measurement system transport measurement system (see SM [34]). The temperature-dependent resistivity $\rho(T)$ is shown in the Fig. 1(a). To rule out the possibility of electrical conduction channels through LP-/HP-LMO, we have measured resistivity of individual layers grown on LSAT substrates which were highly resistive compared to the $SrIrO_3$ semimetallic layer (see SM [34]). The temperature-dependent behavior of magnetization (field cooling) measured at 500 Oe of these bilayer samples are also shown in Fig. 1(b). The first change of slope in the ρ versus T plot of the HP-LMO-SIO sample was found to be around 50 K [defined as T_1, in Fig. 1(a)], which corresponds to weak antilocalization (WAL) to weak localization (WL) crossover usually found in $SrIrO_3$ thin films [36]. The second change of slope near 210 K (defined as T_2), which corresponds to the ferromagnetic to paramagnetic transition of $LaMnO_3$, as shown in Fig. 1(b). Similarly, the change of slope near 120 K (defined as T_3) in electrical transport measurements [see Fig. 1(a)] also corresponds to Curie temperature (T_C) of the LP-LMO layer [see Fig. 1(b)] in the magnetic measurements. A clear shift in the T_C as well as the magnitude of the magnetic moment in both samples are consistent with earlier reports, ascertaining that the disproportion of Mn^{3+} and Mn^{4+} drives $LaMnO_3$ layers to different magnetic orders [23,24]. The oxygen gas atmosphere during the deposition allows oxygen to be absorbed into the lattice, thereby enhancing the formation of Mn^{4+} ions promoting double exchange mediated ferromagnetic ordering in epitaxial HP-LMO thin films [21,23,24]. When the pO_2 during $LaMnO_3$ deposition decreases, this enhances formation of increased Mn^{3+} which has a smaller magnetic moment compared to Mn^{4+} the $LaMnO_3$ layer evolves to an antiferromagnetic ground state. To quantify Mn^{3+} and Mn^{4+}, we have performed XPS measurements on HP- and LP-LMO samples (see SM [34]), which is a surface-sensitive technique. XPS results are in agreement with earlier reports of increased Mn^{4+} content in HP-LMO samples and lower content of Mn^{4+} in LP-LMO samples. Also, to verify the oxygen non-stoichiometry and La/Mn ratio, we have carried out Rutherford backscattering spectroscopy in $LaMnO_3$ thin films grown at different pO_2. The RBS data shows that the HP-/LP-LMO samples are nearly stoichiometric (see SM [34]). The oxygen content in the $LaMnO_3$ thin films are roughly estimated, which has been found to increase for the HP-LMO sample compared to that of the LP-LMO (see SM [34]).

We observed anomalous Hall effect (AHE) in transverse resistance measurement induced by charge-transfer-mediated magnetism at the LMO-SIO interface [35,36]. Transverse resistance was measured in Hall bar configuration as a function of temperature (see SM [34]). The linear high magnetic field contribution are subtracted and plotted as shown in Fig. 1(c). The higher AHE contribution from HP-LMO-SIO compared to LP-LMO-SIO follows our magnetization data as expected in the Fig. 1(b). Further, Fig. 1(d) shows carrier density (n_{2D}) as a function of temperature extracted from the slope at linear part of high magnetic field region whereas Fig. 1(e) shows mobility (μ). The mobility and carrier densities are

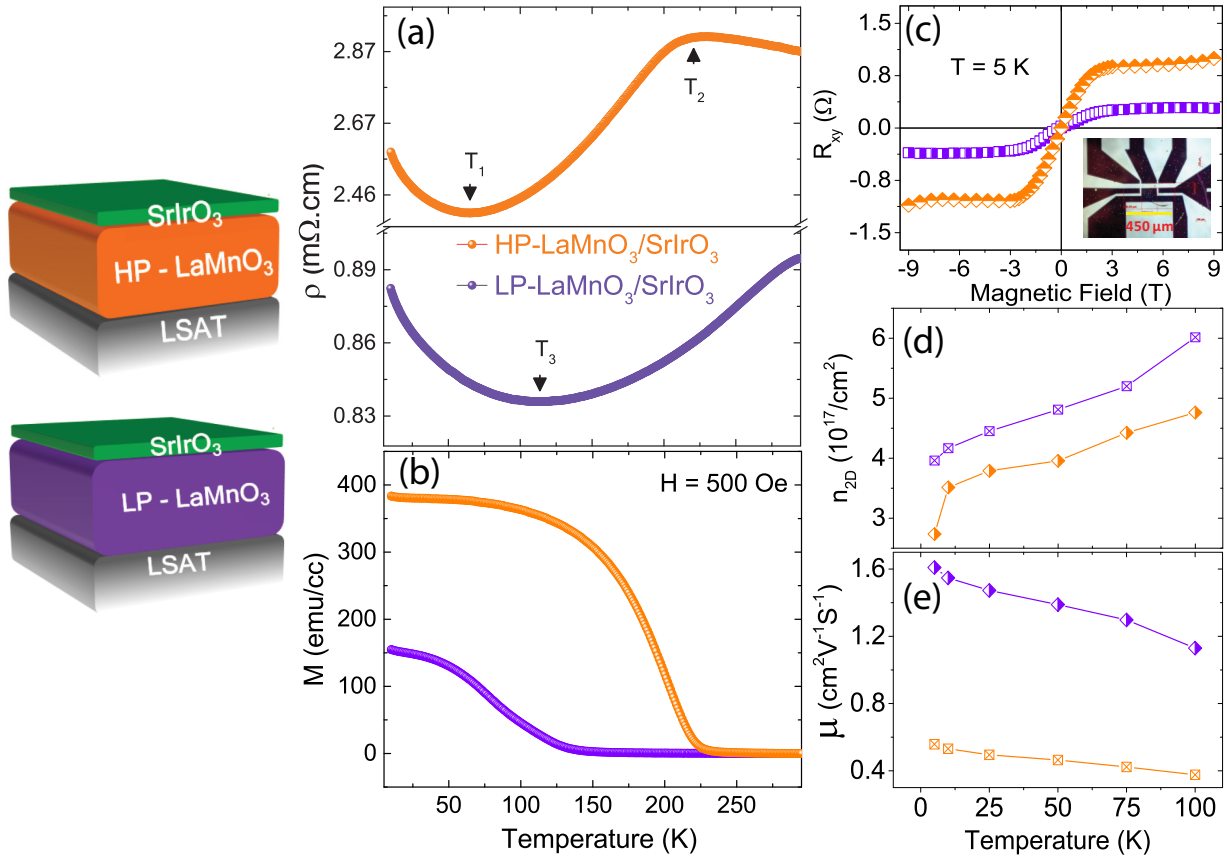

FIG. 1. Schematic image of the layered structure of $LaMnO_3$ deposited at 37.5×10^{-3} mTorr (LP-LMO-SIO) and 37.5 mTorr (HP-LMO-SIO) bilayer samples (left). (a) Temperature dependence of resistivity (ρ) and (b) magnetization (M) at an applied magnetic field of 500 Oe infield-cooled (FC) protocol are demonstrated in (a) and (b), respectively, for HP- and LP-LMO-SIO bilayers. (c) Comparison of LP-/HP-LMO-SIO anomalous Hall effect (AHE) contribution deduced from transverse resistance data by subtracting the linear Hall contribution (Hall bar structure is shown as inset in Fig. 1(c)). (d), (e) Carrier density (n_{2D}) and mobility (μ) of LP/HP-LMO-SIO layer as a function of temperature extracted from Hall measurements, respectively.

comparatively higher in magnitude for the LP-LMO-SIO sample relative to the HP-LMO-SIO sample. In the HP-LMO-SIO, the mobility values are comparable to values reported in literature on LSMO/SIO heterostructures [28], which indicates the magnetic scattering at the LMO-SIO interface. Whereas in LP-LMO-SIO, WAL/WL effects dominate over the magnetic screening by the $LaMnO_3$ under layer.

To further understand the electronic transport behavior and electron spin relaxation mechanism, magnetotransport measurements were carried out on the bilayer samples at different temperatures as shown in Figs. 2(a) and 2(b). The magnetoconductance (MC) measured with an external magnetic field applied perpendicular to the interface showed a negative to positive crossover arising from WAL effects [37]. The in-plane magnetoresistance (see SM [34]) measured at 5 K showed a negative magnetoresistance for both LP/HP-LMO-SIO samples, which is due to dominating orbital contribution [38,39]. Our interest is on the observed crossover in out-of-plane MC, which is dominant at low temperatures and becomes weaker with an increase in temperature and vanishes near 100 K and 125 K for LP-/HP-LMO-SIO, respectively. At low magnetic fields, the negative MC component is dominant, and at high magnetic fields the positive MC component is dominant. Negative MC (at temperatures below 10 K) reported in ultrathin $SrIrO_3$ films grown on compressively strained LSAT and STO substrates arises due to the competition between WL and strong spin-orbit-coupling-based WAL [35]. Usually, from various reports, the crossover from negative to positive MC arises in ultrathin $SrIrO_3$ thin films in the temperature range of 7–10 K [14,40,41]. However, we observed a crossover in MC at low magnetic fields in the temperature range of 100 to 125 K for both HP-/LP-LMO-SIO, as shown in Figs. 2(a) and 2(b). $SrIrO_3$ grown on HP- and LP-LMO show a different temperature dependence in the crossover of MC from positive MC to negative MC. In addition, the shape of MC has also been found to change for both samples. To investigate this scenario in terms of spin-orbit coupling in the LP- and HP-LMO-SIO layers, we used the Hikami-Larkin-Nagaoka (HLN) equation [42] to fit the MC data.

$$\frac{\Delta\sigma(B)}{G_0} = -\Psi\left(\frac{1}{2}+\frac{B_e}{B}\right) + \frac{3}{2}\Psi\left(\frac{1}{2}+\frac{B_i+B_{so}}{B}\right) - \frac{1}{2}\Psi\left(\frac{1}{2}+\frac{B_i}{B}\right) - \ln\left(\frac{B_i+B_{so}}{B_e}\right) - \frac{1}{2}\ln\left(\frac{B_i+B_{so}}{B_i}\right). \quad (1)$$

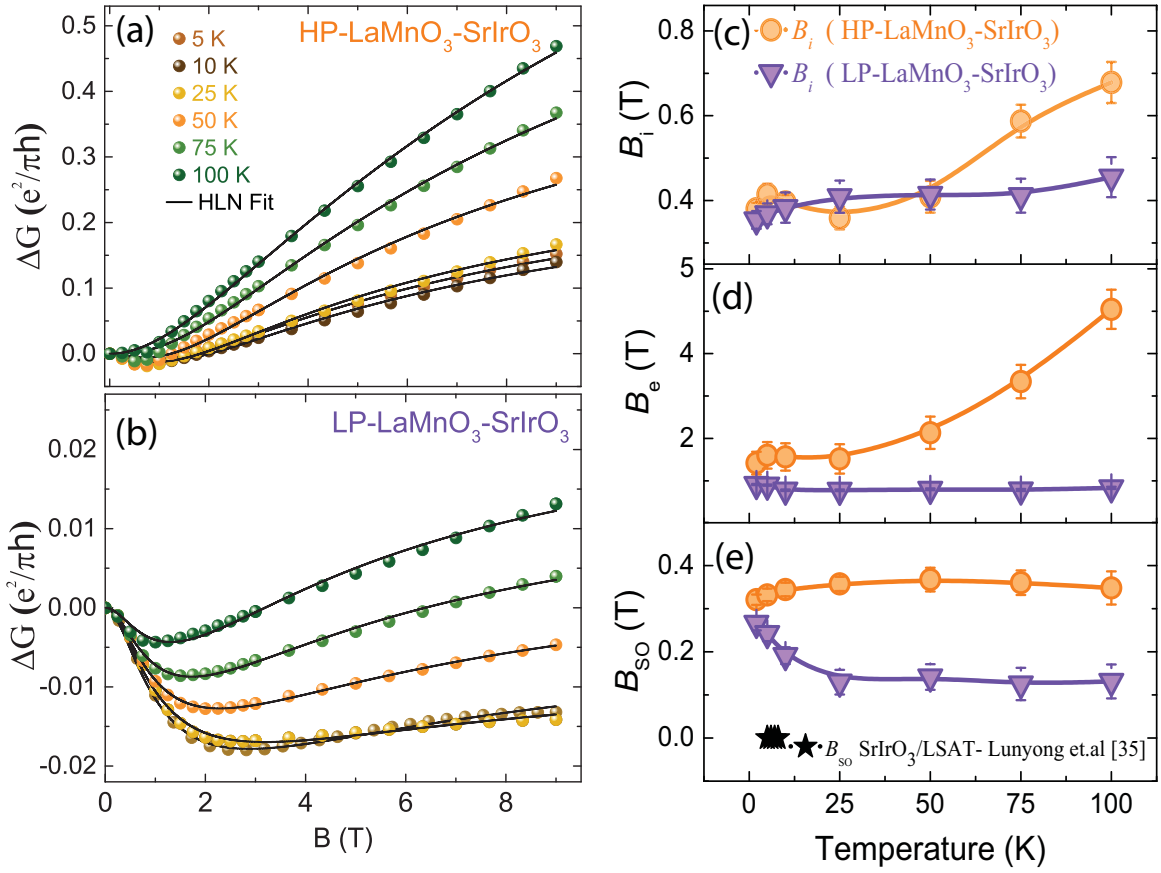

FIG. 2. (a), (b) Experimental magnetoconductance (ΔG) data (closed colored symbols) as a function of magnetic field B ($\perp$) interface; measured for different temperatures fitted (solid black curve) by the Hikami-Larkin-Nagaoka equation for HP-/LP-LMO-SIO samples, respectively. Evolution of fitting parameters B_i (c), B_e (d) and B_{SO} (e) as a function of temperature for HP-/LP-LMO-SIO samples. The reported $SrIrO_3$/LSAT [35] has also been plotted for comparison in (e).

In Eq. (1), ψ is digamma function and G_0 is the universal conductance constant; 1.2 x 10-5 S. B_e, B_i and B_{so} represent effective fields of elastic, inelastic, and spin-orbit coupling induced scattering terms, respectively. The HLN equation best describes the competition between spin-orbit coupling and WL. MC behavior in LP/HP-LMO-SIO is in good agreement with the HLN model in the temperature range between 5 K and 100 K. We could extract different scattering parameters as a function of temperature, as shown in Figs. 2(c)–2(e). The magnitude of these parameters obtained for our samples is one order of magnitude higher in comparison to the direct $SrIrO_3$ layer grown on LSAT with similar deposition conditions.

The elastic scattering field (B_e) which is one order of magnitude higher compared to B_i and B_{so} fields which are in agreement with the fact that the electronic transport is dominated by two-dimensional (2D) WL [43]. We could see that the parameter B_i has comparable magnitudes in both LP-/HP-LMO-SIO samples and follows a similar temperature-dependent trend. However, HP-LMO-SIO has higher B_e values compared to the LP-LMO-SIO, which agrees with the interaction of conduction electrons in $SrIrO_3$ with the magnetic moment of interfacial Mn spins. In HP-LMO-SIO. the magnetic moment is higher compared to LP-LMO-SIO, hence the higher magnitude of B_e in the HP-LMO-SIO sample can be attributed to electrons screened due to interfacial Mn spins.

In the case of B_{so}, both samples exhibit different behaviors as function of temperature, and the LP-LMO-SIO show a decrease in B_{so} and saturates above 25 K. Whereas the B_{so} parameter increases till 25 K and saturates afterward for the HP-LMO-SIO. The magnitude of B_{so} is one order higher compared to $SrIrO_3$ directly grown on LSAT. The B_{so} parameter is directly related to the induced spin-orbit coupling at the $SrIrO_3$ layer. Therefore, the temperature-dependent trend of B_{so} and B_e parameters point to the fact that the Mn spins at the interface and their magnetic moment plays a vital role in tuning the spin-orbit coupling at the interface.

The role of Mn spins on the scattering of electrons at the interface could be arising from an internal electric field generated due to charge transfer from Ir ions to Mn ions. A recent report of Huang *et al.* on $LaMnO_3/SrIrO_3$ superlattices showed the internal electric field arising from the strain induced in the Ir-O-Ir bond angle, which is having a Rashba-like character, at the $LaMnO_3$-$SrIrO_3$ interface [44]. Rashba interactions caused by broken mirror symmetry and, in particular, by the associated electric field perpendicular to the $SrIrO_3$ interface induces orbital and lattice polarization due to asymmetric interfacial structure of $LaMnO_3$-$SrIrO_3$ interface [44]. The temperature-dependent Rashba spin-orbit coupling

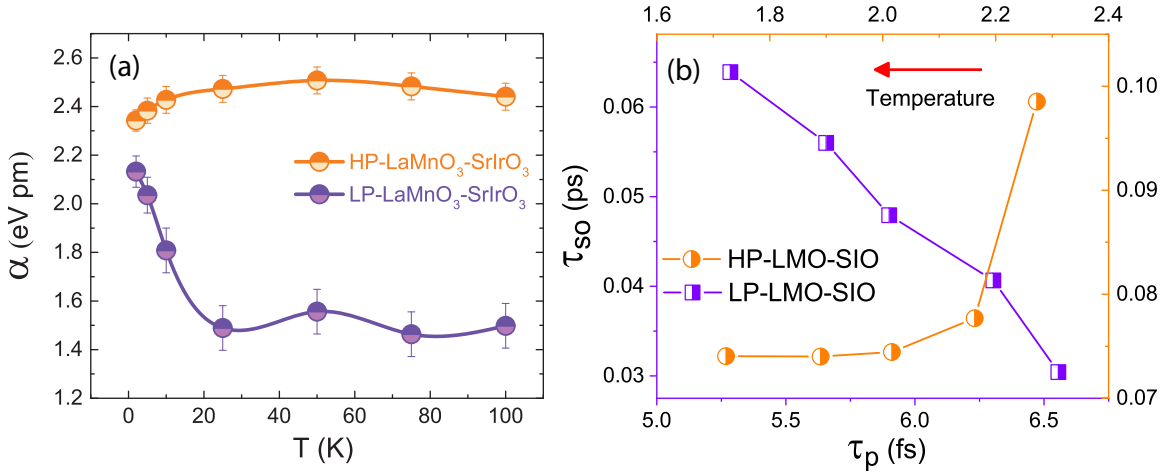

FIG. 3. (a) Rashba spin-orbit coupling (α) extracted from B_{SO} values using Eq. 2 is shown as a function of temperature for HP-/LP-LMO-SIO samples. (b) Spin relaxation (τ_{so}) versus momentum scattering timescale (τ_p) for HP-/LP-LMO-SIO as a function of temperature.

has earlier studied in several semiconductor heterostructures [45]. The higher-order terms in Rashba spin-orbit Hamiltonian are found to be the origin of this temperature dependence [46]. In case of $SrIrO_3$, temperature dependence of Rashba spin-orbit coupling is reported to arise from changes in the g factor, which is affected by temperature [35]. To investigate the role of Rashba spin-orbit coupling in magnetotransport at the $LaMnO_3$-$SrIrO_3$ interface, the Rashba coefficients for LP-/HP-LMO-SIO were obtained as a function of temperature from B_{so} parameter. The B_{so} parameter is related to the Rashba spin-orbit coupling coefficient as [35,47,48]

$$\alpha = \frac{(e\hbar^3 B_{so})^{\frac{1}{2}}}{m^*}. \tag{2}$$

Here m^* is the effective mass, in case of $SrIrO_3$ $m^* \sim 7m_o$ (m_o: the mass of an electron) [35,47]. e is the elementary charge and $\hbar$ is the reduced Planck's constant. The Rashba spin-orbit coupling coefficients (α, eVpm) are plotted as a function of temperature for both samples, as shown in Fig. 3(a). The value of α has been obtained for $SrIrO_3$ thin films grown on compressively strained LSAT (001) and STO (001) substrates by Zhang *et al.* [35], which exactly matches with the single $SrIrO_3$ layer grown on LSAT substrates. In both LP-/HP-LMO-SIO samples, the Rashba spin-orbit coupling coefficient is found to be even higher, with a 10% increase compared to $SrIrO_3$ directly grown on LSAT substrates. This enhanced Rashba spin-orbit coupling is due to charge transfer, depending on the valence state of underlying Mn, which shows different temperature dependencies at low temperatures. Moreover, HP-LMO-SIO shows a weak temperature dependence compared to LP-LMO-SIO at low temperatures though both saturates at high temperatures (above 25 K). The change in the magnetization over the range of temperature (5 K to 25 K) is quite large in LP-LMO-SIO compared to the HP-LMO-SIO sample as shown in Fig. 1(b). Also, as we know that the spin-orbit field B_{so} parameter depends on the nature of magnetic interface, which can be related to the change in the B_{so} as shown in the Fig. 2(e). We can also notice the large change in the B_{so} in LP-LMO-SIO samples compared to the HP samples below 25 K. Whereas, above 50 K, we could not see any change in B_{so} in the HP-/LP-LMO-SIO, could be due to the thermal effects which suppresses any changes arising from Mn spins. Hence the interfacial coupling between different magnetically ordered $LaMnO_3$ also provides an impact on the coupling between the spin-orbit-coupled state of Ir^{4+}. As we know, changing the growth pressure on $LaMnO_3$ significantly affects the lattice constant of the $LaMnO_3$ layer [21]. $LaMnO_3$ grown under low pO_2 were partially relaxed with the lattice constant $a_{LP} = 0.400$ nm. On the other hand, for thin films grown under oxidizing atmospheres are found to be compressively strained (-0.63%), with lattice constant $a_{HP} = 0.392$ nm (see SM [34]). It has been found that $SrIrO_3$ grown on $LaMnO_3$ is strained due to the strain in $LaMnO_3$ lattice. This may lead to changes in the Ir-O-Ir bond angle (lattice polarization). The IrO_6 octahedral rotation due to strain in the Ir-O-Ir bond angle has also been found to enhance interfacial charge transfer [29], which may enhance the electric field responsible for Rashba spin-orbit coupling.

To get more insights about the influence of interface-induced Rashba spin-orbit coupling in spin relaxation mechanism in these bilayers, we considered two commonly observed mechanisms: the D'yakonov-Perel (DP) and the Elliot-Yafet (EY) mechanisms [49]. The DP-type spin relaxation arises in systems that lack inversion symmetry, in which the electron spin precesses in an effective magnetic field with its direction changing after each scattering event [50,51]. Depending on whether it is bulk or interface, the DP mechanism has Dresselhaus and Rashba-type contributions, respectively [52,53]. On the other hand, the EY mechanism originates from spin-orbit-coupling-induced spin dephasing due to electron-phonon coupling or interfacial defects [49]. Apart from this in thin films, there could be other contributions to EY mechanism such as scattering events at the grain boundary, oxygen-vacancy-induced defects, and lattice dislocations [54,55]. Both DP and EY mechanisms can be identified by the relation between spin scattering timescale τ_{so} and momentum scattering timescale τ_p. If the τ_{so} scales linearly with τ_p then the dominant mechanism is EY, and if it is inversely proportional, the DP type is the dominant mechanism [49].

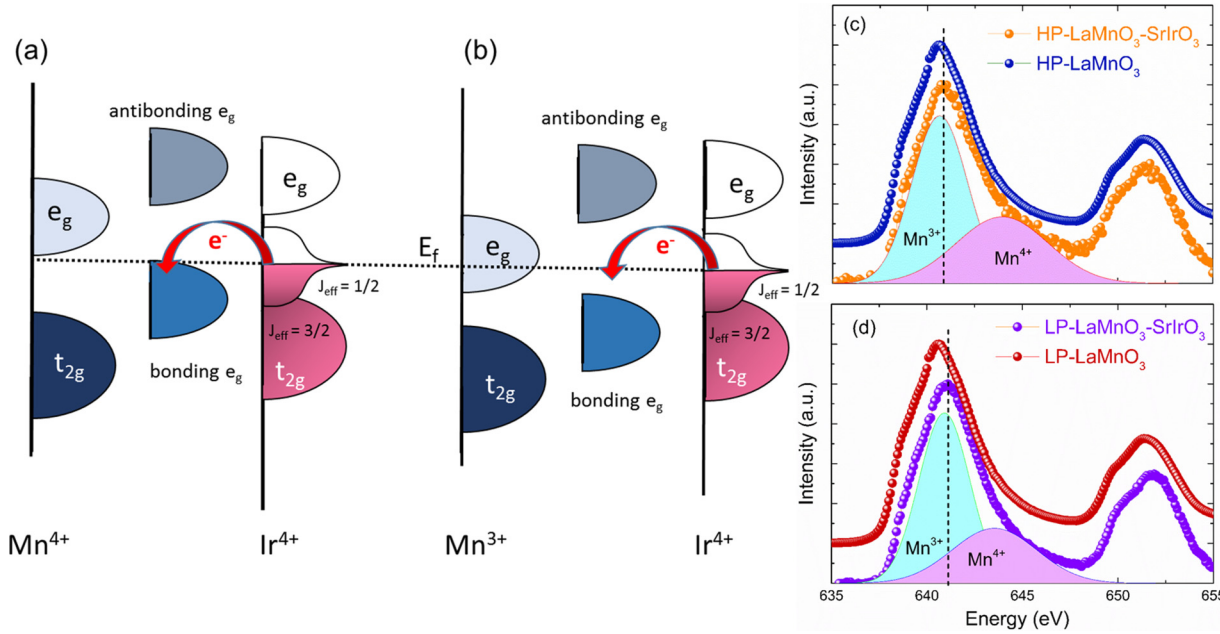

FIG. 4. Schematic representation of charge transfer mechanism for Ir^{4+} to Mn^{4+} (a) and Ir^{4+} to Mn^{3+} (b). (c), (d) XAS spectra around Mn $L_{2,3}$ edge of HP- and LP-LMO-SIO samples along with corresponding HP- and LP-LMO samples without $SrIrO_3$ layer. The respective Mn valence state position, as deconvoluted Mn *L-3* edge is shown for Mn^{3+} and Mn^{4+} in the bilayer as a shaded area (valence states are quantified by XPS spectra analysis (see SM [34]), the shaded area is for representation). The dashed black lines in the figure are guide to the eye based on the shift of the Mn-*L* edge position of LP- and HP-LMO-SIO with their corresponding $LaMnO_3$ samples.

In HP- and LP-LMO-SIO samples the spin relaxation timescale τ_{so} and momentum relaxation (τ_p) timescale were estimated from B_{so} parameter and mobility [49]:

$$\tau_{so} = \frac{\hbar}{4eB_{so}D}, \tag{3a}$$

$$\tau_p = \frac{m^*\mu}{e}. \tag{3b}$$

Here D is the diffusion coefficient, which is related to Fermi energy as $D = 2\mu E_F/3e$ for degenerate systems [40]. The D can be estimated from $D = v_F^2\tau_p/2$, $v_F = \hbar k_F/m^*$, $k_F = \sqrt{2\pi n_{2D}}$, where v_F is the Fermi velocity, k_F is the Fermi wave vector, and n_{2D} is the carrier density. τ_{so} and τ_p are plotted using Eqs. (3a) and (3b), as shown in Fig. 3(b) to investigate the relations between them. In HP-LMO-SIO samples, the EY-type spin relaxation mechanism dominates at lower temperatures according to the τ_{so} and τ_p dependence as shown in Fig. 3, which eventually deviates to DP-type mechanism at higher temperatures. The dominance of EY-type spin relaxation mechanism in HP-LMO-SIO samples arises from interfacial defects and screening from Mn magnetic moments present at the interface. On the other hand, we found that τ_{so} is inversely proportional to τ_p in the LP-LMO-SIO sample, which is supposed to be a DP-type spin relaxation mechanism. However, the magnitude of τ_p is weakly temperature dependent in both HP-/LP-LMO-SIO samples and is difficult to identify the spin relaxation mechanism as an ideal DP or EY type. This discrepancy of spin relaxation mechanism in our bilayer samples could be attributed to the influence of an induced magnetic order at the $LaMnO_3$-$SrIrO_3$ interface. Further studies with other complimentary experimental techniques are required to understand the spin dynamics of $LaMnO_3$-$SrIrO_3$ interface.

In the case of bulk $LaMnO_3$, under the crystal field created by oxygen $2p$ states in octahedrally coordinated MnO_6, the five Mn $3d$ levels split into low-energy t_{2g} triplet and high-energy e_g doublet levels, as sketched in Figs. 4(a) and 4(b). In general, in hole-doped $LaMnO_3$ systems, the Mn ions are in a mixed trivalent ($3d^4$) and tetravalent ($3d^3$) states [30]. In the case of Mn^{4+} the e_g orbitals are empty and singly occupied for Mn^{3+}. In our case, we have mixed-valence states with varying amounts of Mn^{3+} and Mn^{4+} for HP- and LP-LMO-SIO samples. Further, the e_g states of Mn^{3+} and Mn^{4+} couples with interfacial e_g states of Ir^{4+} to give rise to molecular orbitals with energetically lower lying bonding and upper lying antibonding levels [30]. This coupling of $e_g(3z^2\text{-}r^2$ bonding orbital) states at the interface promotes charge transfer from Ir^{4+} to Mn^{3+} and Mn^{4+} states. To experimentally ascertain the charge transfer at the interface, XAS study in total-electron-yield (TEY) mode has been performed on HP- and LPLMO-SIO bilayer samples and, HP- and LP-LMO without $SrIrO_3$ layer as illustrated in Figs. 4(c) and 4(d). At first, XAS data rules out the existence of any other valence states other than Mn^{3+} and Mn^{4+} in $LaMnO_3$. The LP-LMO-SIO bilayer sample shows a shift of 1.54 eV toward higher energy compared to LP-LMO and similarly HP-LMO-SIO shows a shift of 0.25 eV compared to HP-LMO. The LP-LMO-SIO sample shows a pronounced shift due to a predominant concentration of Mn^{3+} ions over Mn^{4+} ions as seen in XPS spectra (see SM [34]). Since the Mn^{3+} bonding orbital lies much lower to the Fermi level compared to Mn^{4+} (sketched in Figs. 4(a) and 4(b)], the Mn^{3+} contributes predominantly to the charge transfer process; this observation is in compliance with recently

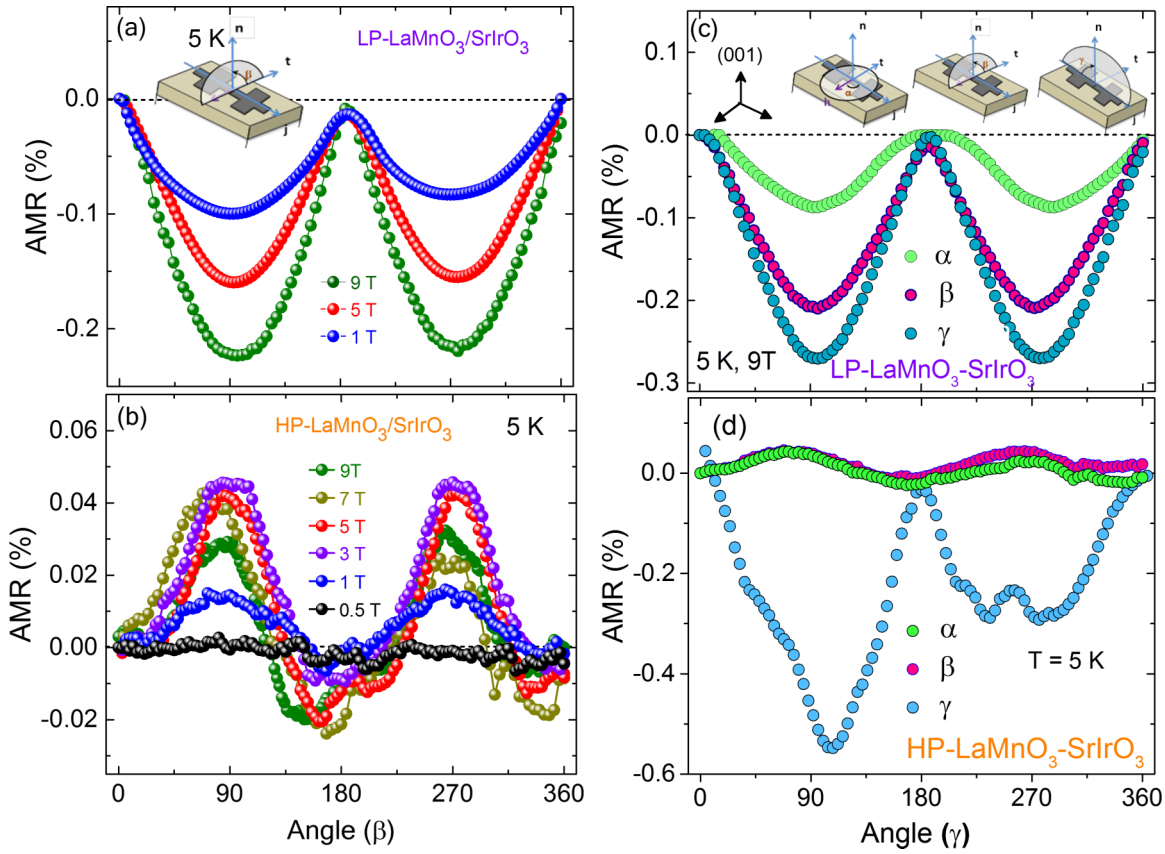

FIG. 5. (a), (b) The angle-dependent magnetoresistance (ADMR) measurements carried out as a function of the magnetic field for LP- and HP- LMO-SIO samples, respectively, in β rotational plane (schematic of the β rotational measurement configuration in inset). (c), (d) ADMR measurements as a function of different rotational configurations. The rotational planes are shown as an inset in (c) with respect to crystallographic orientation. The angles α, β, γ are defined as the angle subtended between the current direction j with respect to the magnetic field rotation, and n is represented as a direction cosine normal to the surface. α points to the in-plane (IP) rotation of magnetic field with respect to n. β represent out of plane (OOP) rotation direction lying in the plane perpendicular to the current direction j. γ shows the OOP direction with respect to the current direction plane j.

reported $LaMnO_3/SrIrO_3$ superlattices [44]. Also, the charge transfer has two competing contributions arising from strain in IrO_6 octahedra and due to overlap of low-lying e_g bonding orbitals in Mn^{3+} compared to Mn^{4+} at the interface. Our data shows the charge transfer being responsible for EY-type spin relaxation mechanisms in LMO-SIO interfaces.

We have further carried out ADMR measurements to understand the charge-transfer effects on transport behavior in $SrIrO_3$ due to the interfacial Mn spins in HP- and LP-LMO-SIO samples. The $\text{ADMR}(\%) = [\text{R}(\alpha, \beta, \gamma) - R(0))/R(0)]$ investigated as a function of magnetic field and rotational planes at 5 K, where $R(0)$ is the resistance when magnetic field is normal to the sample surface and $R(\alpha, \beta, \gamma)$ is the resistance with respect to each rotational plane (α, β, γ) as shown in the Fig. 5(c) inset. The bilayers are grown epitaxially over a cubic substrate which is expected to show a fourfold symmetry depending on magneto crystalline anisotropy in $SrIrO_3$ [56,57], but in our case we observed a twofold symmetry in ADMR measurements for both LP-/HP-LMO-SIO samples. The observed ADMR signals showed a phase shift of $\pi/2$ for LP-LMO-SIO compared to the HP-LMO-SIO sample. In particular, we observe a distinct magnetoresistance trend in the LP-LMO-SIO sample as $[\text{MR}(\gamma) > \text{MR}(\beta) \gg \text{MR}(\alpha)]$, Fig. 5(c) compared to SMR, which has the form $[\text{MR}(\alpha)=\text{MR}(\beta) \gg \text{MR}(\gamma)]$. This ADMR trend of LP-LMO-SIO does not comply with the conditions meant for anisotropic magnetoresistance (AMR), i.e., $[\text{MR}(\alpha)= \text{MR}(\gamma) \gg \text{MR}(\beta)]$. This is also distinct from the recently reported proximity-induced magnetoresistance (PMR) for which the condition is $[\text{MR}(\beta) = \text{MR}(\gamma) \gg \text{MR}(\alpha)]$ [58]. On the other hand, in the case of the HP-LMO-SIO, the trend points to $[\text{MR}(\gamma) > \text{MR}(\beta) \approx \text{MR}(\alpha)]$, Fig. 5(d), this does not resemble any above-mentioned magnetoresistance models. Additionally, the observed ADMR data is quite different from reported MPEs in SMR of ferromagnets (FM) [59] and MPE in SMR of antiferromagnets [60].

$LaMnO_3$ orients as an A-type antiferromagnet in bulk and thin films, as shown in earlier reports using scanning SQUID microscopy [20]. In the case of fully relaxed $LaMnO_3$ thin films, the intraplane exchange interaction is ferromagnetic, whereas the interplane exchange interaction is antiferromagnetic, which may lead to an A-type antiferromagnetic ordering. However, in our case we have strained epitaxial films that have ferromagnetic exchange interactions that result in overall ferromagnetic ordering. In LP-LMO-SIO samples, we expect the overall magnetic ordering is

antiferromagnetic and the trend and magnitude of ADMR correspond to the effect of induced magnetism at the interface, such that magnetization rotation is reflected in the ADMR data. This observation was in agreement with the field-dependent changes in ADMR signals of LP-/HP-LMO-SIO samples. In the case of $LaMnO_3$-$SrIrO_3$ bilayers, there is a mixed effect from SMR as well as proximity-induced magnetism (MPE) arising from charge transfer at the interface. The field-dependent ADMR [Figs. 5(a) and 5(b)] in HP-LMO-SIO sample show an amplified signal at 3 T, and it decreases with increasing magnetic field strength, which suggests the existence of competing domains which percolates with increasing magnetic field in $LaMnO_3$. In the LP-LMO-SIO sample case, we have observed a nonsaturating ADMR which is due to the presence of antiferromagnetic order that prevails with the magnetic field and MPE being a dominant contribution arising from induced magnetism in the $LaMnO_3$-$SrIrO_3$ interface. Further experimental and theoretical studies are required to understand the domain structure of $LaMnO_3$ with MPE effects to extract the spin-charge conversion at $LaMnO_3$-$SrIrO_3$ interface using a theoretical macrospin model to explore such a complicated magnetic structure.

III. CONCLUSION

In summary, we have explored the 3*d*-5*d* interface interactions through tunability of the magnetic order in $LaMnO_3$ by varying the oxygen partial pressure during $LaMnO_3$ deposition. The x-ray spectroscopy measurements indicate that the changes in the magnetic ordering of $LaMnO_3$ can be attributed to the creation of multiple valence states. A tunable and enhanced Rashba spin-orbit coupling is estimated at LP- and HP-LMO-SIO as a function of temperature from MC measurements that arises from electric field generated due to strain in the Ir-O-Ir bond angle as well as interfacial charge transfer from Ir^{4+} to Mn^{3+} and Mn^{4+}. The spin-relaxation mechanism at the $LaMnO_3$-$SrIrO_3$ interface is observed to be tunable with magnetic order of the underlying $LaMnO_3$ layer. However, an ideal EY- or DP-type spin-relaxation mechanisms cannot be identified in our samples since the τ_p does not change significantly with the temperature. The contribution of Mn spins in $LaMnO_3$ on electronic transport was further probed using ADMR measurements, which reflects the magnetic order of underlying $LaMnO_3$ and charge-transfer-induced magnetism at the $LaMnO_3$-$SrIrO_3$ interface. The evolution of these phenomena is attributed to the 3*d*-5*d* interface electronic correlation and the Rashba spin-orbit coupling at the $LaMnO_3$-$SrIrO_3$ interface. In conclusion, the present results provide a platform of 3*d*-5*d* oxide interface engineering and raises possibilities in tuning these interface interactions to optimize spin transport in emerging quantum material $SrIrO_3$.

ACKNOWLEDGMENTS

M.S.R. and K.S. would like to acknowledge the Science and Engineering Research Board (SERB) Grant No. EMR/2017/002328 for the financial support. The authors would like to acknowledge Dr. Matthias Opel and Dr. Matthias Althammer of Walther Meissner Institute Garching, Technical University of Munich (TUM) Germany for insightful discussions and suggestions on the modification of the paper. The authors would like to acknowledge Prof. Mahendran and his student Amit Chanda of National University of Singapore (NUS) for their help in measurements. The research at NUS is supported by the Agency for Science, Technology and Research (A*STAR) under its Advanced Manufacturing and Engineering (AME) Individual Research Grant (IRG) (Grant No. A1983c0034), the National University of Singapore (NUS) Academic Research Fund (AcRF Tier 1 Grants No. R-144-000-391-144 and No. R-144-000-403-114) and the Singapore National Research Foundation (NRF) under the Competitive Research Programs (CRP Award No. NRF-CRP15-2015-01). H.J. would like to thank NUS Graduate School of Integrative Science and Engineering (NGS) for fellowship.

[1] J. Nichols, X. Gao, S. Lee, T. L. Meyer, J. W. Freeland, V. Lauter, D. Yi, J. Liu, D. Haskel, J. R. Petrie, E.-J. Guo, A. Herklotz, D. Lee, T. Z. Ward, G. Eres, M. R. Fitzsimmons, and H. N. Lee, Emerging magnetism and anomalous Hall effect in iridate-manganite heterostructures, Nat. Commun. **7**, 12721 (2016).

[2] A. Ohtomo and H. Hwang, A high-mobility electron gas at the $LaAlO_3/SrTiO_3$ heterointerface, Nature **427**, 423 (2004).

[3] K. S. Takahashi, M. Kawasaki, and Y. Tokura, Interface ferromagnetism in oxide superlattices of $CaMnO_3/CaRuO_3$, Appl. Phys. Lett. **79**, 1324 (2001).

[4] C. Cen, S. Thiel, G. Hammerl, C. W. Schneider, K. E. Andersen, C. S. Hellberg, J. Mannhart, and J. Levy, Nanoscale control of an interfacial metal-insulator transition at room temperature, Nat. Mater. **7**, 298 (2008).

[5] J. Hoffman, I. C. Tung, B. B. Nelson-Cheeseman, M. Liu, J. W. Freeland, and A. Bhattacharya, Charge transfer and interfacial magnetism in $(LaNiO_3)_n/(LaMnO_3)_2$ superlattices, Phys. Rev. B **88**, 144411 (2013).

[6] G. J. Omar, M. Li, X. Chi, Z. Huang, Z. S. Lim, S. Prakash, S. Zeng, C. Li, X. Yu, C. Tang, D. Song, A. Rusydi, T. Venkatesan, S. J. Pennycook, and A. Ariando, Characteristic lengths of interlayer charge transfer in correlated oxide heterostructures, Nano Lett. **20**, 2493 (2020).

[7] A. Manchon, H. C. Koo, J. Nitta, S. M. Frolov, and R. A. Duine, New perspectives for rashba spin-orbit coupling, Nat. Mater. **14**, 871 (2015).

[8] A. Soumyanarayanan, N. Reyren, A. Fert, and C. Panagopoulos, Emergent phenomena induced by spin-orbit coupling at surfaces and interfaces, Nature **539**, 509 (2016).

[9] Y. A. Bychkov and E. I. Rashba, Oscillatory effects and the magnetic susceptibility of carriers in inversion layers, J. Phys. C: Solid State Phys. **17**, 6039 (1984).

[10] H. Watanabe, T. Shirakawa, and S. Yunoki, Microscopic Study of a Spin-Orbit-Induced Mott Insulator in Ir Oxides, Phys. Rev. Lett. **105**, 216410 (2010).

[11] T. Takayama, A. N. Yaresko, and H. Takagi, Monoclinic SrIrO3—a dirac semimetal produced by non-symmorphic

symmetry and spin–orbit coupling, J. Phys.: Condens. Matter **31**, 074001 (2018).

[12] W. Witczak-Krempa, G. Chen, Y. B. Kim, and L. Balents, Correlated quantum phenomena in the strong spin-orbit regime, Annu. Rev. Condens. Matter Phys. **5**, 57 (2014).

[13] B. J. Kim, H. Ohsumi, T. Komesu, S. Sakai, T. Morita, H. Takagi, and T. Arima, Phase-sensitive observation of a spin-orbital Mott state in Sr2IrO4, Science **323**, 1329 (2009).

[14] A. Biswas, K.-S. Kim, and Y. H. Jeong, Metal insulator transitions in perovskite $SrIrO_3$ thin films, J. Appl. Phys. **116**, 213704 (2014).

[15] A. Biswas and Y. H. Jeong, Growth and engineering of perovskite $SrIrO_3$ thin films, Current Appl. Phys. **17**, 605 (2017).

[16] A. Biswas, K.-S. Kim, and Y. H. Jeong, Emergence of non-fermi liquid behaviors in 5d perovskite $SrIrO_3$ thin films: Interplay between correlation, disorder, and spin-orbit coupling, J. Magn. Magn. Mater. **400**, 36 (2016).

[17] J. Töpfer and J. Goodenough, $LaMnO_3 + \delta$ revisited, J. Solid State Chem. **130**, 117 (1997).

[18] Q. Huang, A. Santoro, J. W. Lynn, R. W. Erwin, J. A. Borchers, J. L. Peng, and R. L. Greene, Structure and magnetic order in undoped lanthanum manganite, Phys. Rev. B **55**, 14987 (1997).

[19] C. Ritter, M. R. Ibarra, J. M. De Teresa, P. A. Algarabel, C. Marquina, J. Blasco, J. García, S. Oseroff, and S.-W. Cheong, Influence of oxygen content on the structural, magnetotransport, and magnetic properties of $LaMnO_{3+\delta}$, Phys. Rev. B **56**, 8902 (1997).

[20] X. R. Wang, C. J. Li, W. M. Lü, T. R. Paudel, D. P. Leusink, M. Hoek, N. Poccia, A. Vailionis, T. Venkatesan, J. M. D. Coey, E. Y. Tsymbal, A. Ariando, and H. Hilgenkamp, Imaging and control of ferromagnetism in $LaMnO_3/SrTiO_3$ heterostructures, Science **349**, 716 (2015).

[21] J. Roqueta, A. Pomar, L. Balcells, C. Frontera, S. Valencia, R. Abrudan, B. Bozzo, Z. Konstantinović, J. Santiso, and B. Martínez, Strain-engineered ferromagnetism in $LaMnO_3$ thin films, Cryst. Growth Des. **15**, 5332 (2015).

[22] L. Wu, C. Li, M. Chen, Y. Zhang, K. Han, S. Zeng, X. Liu, J. Ma, C. Liu, J. Chen, J. Zhang, Ariando, T. V. Venkatesan, S. J. Pennycook, J. M. D. Coey, L. Shen, J. Ma, X. R. Wang, and C.-W. Nan, Interface-induced enhancement of ferromagnetism in insulating $LaMnO_3$ ultrathin films, ACS Appl. Mater. Interfaces **9**, 44931 (2017).

[23] A. M. Zhang, W. C. Zhang, X. S. Wu, and J. G. Lin, Abnormal enhancement of ferromagnetism for $LaMnO_3 + \delta$ thin films with decreasing oxygen pressure, AIP Adv. **7**, 055837 (2017).

[24] I. Marozau, P. T. Das, M. Döbeli, J. G. Storey, M. A. Uribe-Laverde, S. Das, C. Wang, M. Rössle, and C. Bernhard, Influence of La and Mn vacancies on the electronic and magnetic properties of $LaMnO_3$ thin films grown by pulsed laser deposition, Phys. Rev. B **89**, 174422 (2014).

[25] X. Liu, M. Kotiuga, H.-S. Kim, A. T. N'Diaye, Y. Choi, Q. Zhang, Y. Cao, M. Kareev, F. Wen, B. Pal, J. W. Freeland, L. Gu, D. Haskel, P. Shafer, E. Arenholz, K. Haule, D. Vanderbilt, K. M. Rabe, and J. Chakhalian, Interfacial charge-transfer Mott state in iridaten superlattices, Proc. Natl. Acad. Sci. **116**, 19863 (2019).

[26] D. Yi, C. L. Flint, P. P. Balakrishnan, K. Mahalingam, B. Urwin, A. Vailionis, A. T. N'Diaye, P. Shafer, E. Arenholz, Y. Choi, K. H. Stone, J.-H. Chu, B. M. Howe, J. Liu, I. R. Fisher, and Y. Suzuki, Tuning Perpendicular Magnetic Anisotropy by Oxygen Octahedral Rotations in $(La_{1-x}Sr_xMnO_3)/(SrIrO_3)$ Superlattices, Phys. Rev. Lett. **119**, 077201 (2017).

[27] Y. Li, J. Zhou, and D. Wu, Metal-insulator transition of $LaNiO_3$ films in $LaNiO_3/SrIrO_3$ heterostructures, ACS Appl. Mater. Interfaces **11**, 3565 (2019).

[28] Y. Li, L. Zhang, Q. Zhang, C. Li, T. Yang, Y. Deng, L. Gu, and D. Wu, Emergent topological Hall effect in $La_{0.7}Sr_{0.3}MnO_3/SrIrO_3$ heterostructures, ACS Appl. Mater. Interfaces **11**, 21268 (2019).

[29] S. Okamoto, J. Nichols, C. Sohn, S. Y. Kim, T. W. Noh, and H. N. Lee, Charge transfer in iridate-manganite superlattices, Nano Lett. **17**, 2126 (2017).

[30] T. Yu, B. Deng, L. Zhou, P. Chen, Q. Liu, C. Wang, X. Ning, J. Zhou, Z. Bian, Z. Luo, C. Qiu, X.-Q. Shi, and H. He, Polarity and spin-orbit coupling induced strong interfacial exchange coupling: An asymmetric charge transfer in iridate-manganite heterostructure, ACS Appl. Mater. Interfaces **11**, 44837 (2019).

[31] M. Isasa, S. Vélez, E. Sagasta, A. Bedoya-Pinto, N. Dix, F. Sánchez, L. E. Hueso, J. Fontcuberta, and F. Casanova, Spin Hall Magnetoresistance as a Probe for Surface Magnetization in $Pt/CoFe_2O_4$ Bilayers, Phys. Rev. Appl. **6**, 034007 (2016).

[32] A. Aqeel, N. Vlietstra, A. Roy, M. Mostovoy, B. J. van Wees, and T. T. M. Palstra, Electrical detection of spiral spin structures in $Pt|Cu_2OSeO_3$ heterostructures, Phys. Rev. B **94**, 134418 (2016).

[33] A. S. Patri, K. Hwang, H.-W. Lee, and Y. B. Kim, Theory of large intrinsic spin Hall effect in iridate semimetals, Sci. Rep. **8**, 8052 (2018).

[34] See Supplemental Material at http://link.aps.org/supplemental/10.1103/PhysRevB.102.125145 for sample preparation method, structural and morphological characterization, $LaMnO_3$ controlled sample ρ v/s t measurements, basic transport measurements (IP − OOP magnetoresistance and Hall measurements), x-ray photo-electron spectroscopy and Rutherford back scattering of $LaMnO_3$ thin films.

[35] L. Zhang, Y. B. Chen, B. Zhang, J. Zhou, S. Zhang, Z. Gu, S. Yao, and Y. Chen, Sensitively temperature-dependent spin-orbit coupling in $SrIrO_3$ thin films, J. Phys. Soc. Jpn. **83**, 054707 (2014).

[36] L. Zhang, Q. Liang, Y. Xiong, B. Zhang, L. Gao, H. Li, Y. B. Chen, J. Zhou, S.-T. Zhang, Z.-B. Gu, S.-h. Yao, Z. Wang, Y. Lin, and Y.-F. Chen, Tunable semimetallic state in compressive-strained $SrIrO_3$ films revealed by transport behavior, Phys. Rev. B **91**, 035110 (2015).

[37] N. Nagaosa, J. Sinova, S. Onoda, A. H. MacDonald, and N. P. Ong, Anomalous Hall effect, Rev. Mod. Phys. **82**, 1539 (2010).

[38] F. Hellman, A. Hoffmann, Y. Tserkovnyak, G. S. D. Beach, E. E. Fullerton, C. Leighton, A. H. MacDonald, D. C. Ralph, D. A. Arena, H. A. Dürr, P. Fischer, J. Grollier, J. P. Heremans, T. Jungwirth, A. V. Kimel, B. Koopmans, I. N. Krivorotov, S. J. May, A. K. Petford-Long, J. M. Rondinelli, N. Samarth, I. K. Schuller, A. N. Slavin, M. D. Stiles, O. Tchernyshyov, A. Thiaville, and B. L. Zink, Interface-induced phenomena in magnetism, Rev. Mod. Phys. **89**, 025006 (2017).

[39] W. Knap, C. Skierbiszewski, A. Zduniak, E. Litwin-Staszewska, D. Bertho, F. Kobbi, J. L. Robert, G. E. Pikus, F. G. Pikus, S. V. Iordanskii, V. Mosser, K. Zekentes, and Y. B.

Lyanda-Geller, Weak antilocalization and spin precession in quantum wells, Phys. Rev. B **53**, 3912 (1996).

[40] X. Cai, Y. Ayino, J. Yue, P. Xu, B. Jalan, and V. S. Pribiag, Disentangling spin-orbit coupling and local magnetism in a quasi-two-dimensional electron system, Phys. Rev. B **100**, 081402(R) (2019).

[41] G. M. Minkov, A. V. Germanenko, O. E. Rut, A. A. Sherstobitov, L. E. Golub, B. N. Zvonkov, and M. Willander, Weak antilocalization in quantum wells in tilted magnetic fields, Phys. Rev. B **70**, 155323 (2004).

[42] S. Hikami, A. I. Larkin, and Y. Nagaoka, Spin-orbit interaction and magnetoresistance in the two dimensional random system, Prog. Theor. Phys. **63**, 707 (1980).

[43] M. Pollak and B. Shklovskii, *Hopping Transport in Solids* (Elsevier Science, Amsterdam, 2014).

[44] K. Huang, L. Wu, M. Wang, N. Swain, M. Motapothula, Y. Luo, K. Han, M. Chen, C. Ye, A. J. Yang, H. Xu, D.-c. Qi, A. T. N'Diaye, C. Panagopoulos, D. Primetzhofer, L. Shen, P. Sengupta, J. Ma, Z. Feng, C.-W. Nan, and X. Renshaw Wang, Tailoring magnetic order via atomically stacking 3d/5d electrons to achieve high-performance spintronic devices, Appl. Phys. Rev. **7**, 011401 (2020).

[45] M. A. Leontiadou, K. L. Litvinenko, A. M. Gilbertson, C. R. Pidgeon, W. R. Branford, L. F. Cohen, M. Fearn, T. Ashley, M. T. Emeny, B. N. Murdin, and S. K. Clowes, Experimental determination of the rashba coefficient in InSb/InAlSb quantum wells at zero magnetic field and elevated temperatures, J. Phys.: Condens. Matter **23**, 035801 (2011).

[46] P. S. Eldridge, W. J. H. Leyland, P. G. Lagoudakis, O. Z. Karimov, M. Henini, D. Taylor, R. T. Phillips, and R. T. Harley, All-optical measurement of Rashba coefficient in quantum wells, Phys. Rev. B **77**, 125344 (2008).

[47] D. N. Basov, R. D. Averitt, D. van der Marel, M. Dressel, and K. Haule, Electrodynamics of correlated electron materials, Rev. Mod. Phys. **83**, 471 (2011).

[48] C. Schierholz, T. Matsuyama, U. Merkt, and G. Meier, Weak localization and spin splitting in inversion layers on *p*-type InAs, Phys. Rev. B **70**, 233311 (2004).

[49] I. Žutić, J. Fabian, and S. Das Sarma, Spintronics: Fundamentals and applications, Rev. Mod. Phys. **76**, 323 (2004).

[50] M. I. D'yakonov, Spin orientation of electrons associated with the interband absorption of light in semiconductors, Zh. Eksp. Teor. Fiz. **60**, 1954 (1971) [Sov. Phys. JETP **33**, 1053 (1971)].

[51] M. I. D'yakonov, Spin relaxation of two-dimensional electrons in non-centrosymmetric semiconductors, Sov. Phys. Semicond. **20**, 110 (1986).

[52] P. D. Dresselhaus, C. M. A. Papavassiliou, R. G. Wheeler, and R. N. Sacks, Observation of Spin Precession in GaAs Inversion Layers Using Antilocalization, Phys. Rev. Lett. **68**, 106 (1992).

[53] A. D. Caviglia, M. Gabay, S. Gariglio, N. Reyren, C. Cancellieri, and J.-M. Triscone, Tunable Rashba Spin-Orbit Interaction at Oxide Interfaces, Phys. Rev. Lett. **104**, 126803 (2010).

[54] R. J. Elliott, Theory of the effect of spin-orbit coupling on magnetic resonance in some semiconductors, Phys. Rev. **96**, 266 (1954).

[55] F. Seitz and D. Turnbull, *Solid State Physics: Advances in Research and Applications*, Vol. 14 (Academic Press, New York, 1963).

[56] D. Yi, J. Liu, S.-L. Hsu, L. Zhang, Y. Choi, J.-W. Kim, Z. Chen, J. D. Clarkson, C. R. Serrao, E. Arenholz, P. J. Ryan, H. Xu, R. J. Birgeneau, and R. Ramesh, Atomic-scale control of magnetic anisotropy via novel spin–orbit coupling effect in $La\frac{2}{3}Sr\frac{1}{3}MnO_3/SrIrO_3$ superlattices, Proc. Natl. Acad. Sci. **113**, 6397 (2016).

[57] Z. S. Lim, C. Li, X. Chi, G. J. Omar, H. H. Ma, Z. Huang, S. Zeng, P. Yang, T. Venkatesan, A. Rusydi, S. J. Pennycook, and A. Ariando, Magnetic anisotropy of a quasi two-dimensional canted antiferromagnet, Nano Lett. **20**, 1890 (2020).

[58] K. Takiguchi, L. Duc Anh, T. Chiba, T. Koyama, D. Chiba, and M. Tanaka, Giant gate controlled proximity magnetoresistance in semiconductor based ferromagnetic nonmagnetic bilayers, Nat. Phys. **15**, 1134 (2019).

[59] X. Zhou, L. Ma, Z. Shi, W. J. Fan, J.-G. Zheng, R. F. L. Evans, and S. M. Zhou, Magnetotransport in metal/insulating-ferromagnet heterostructures: Spin Hall magnetoresistance or magnetic proximity effect, Phys. Rev. B **92**, 060402(R) (2015).

[60] Y. Cheng, S. Yu, A. S. Ahmed, M. Zhu, Y. Rao, M. Ghazisaeidi, J. Hwang, and F. Yang, Anisotropic magnetoresistance and nontrivial spin Hall magnetoresistance in $Pt/\alpha-Fe_2O_3$ bilayers, Phys. Rev. B **100**, 220408(R) (2019).